JOURNAL OF GEOPHYSICAL RESEARCH, VOL. 111, B12201, doi:10.1029/2005JB004169, 2006

Potential for carbon dioxide sequestration in flood basalts

B. Peter McGrail,[1] H. Todd Schaef,[1] Anita M. Ho,[2] Yi-Ju Chien,[1] James J. Dooley,[3] and Casie L. Davidson[4]

Received 18 November 2005; revised 15 June 2006; accepted 18 August 2006; published 2 December 2006.

[1] Flood basalts are a potentially important host medium for geologic sequestration of anthropogenic CO_2. Most lava flows have flow tops that are porous and permeable and have enormous capacity for storage of CO_2. Interbedded sediment layers and dense low-permeability basalt rock overlying sequential flows may act as effective seals allowing time for mineralization reactions to occur. Laboratory experiments confirm relatively rapid chemical reaction of CO_2-saturated pore water with basalts to form stable carbonate minerals. Calculations suggest a sufficiently short time frame for onset of carbonate precipitation after CO_2 injection that verification of in situ mineralization rates appears feasible in field pilot studies. If proven viable, major flood basalts in the United States and India would provide significant additional CO_2 storage capacity and additional geologic sequestration options in certain regions where more conventional storage options are limited.

Citation: McGrail, B. P., H. T. Schaef, A. M. Ho, Y.-J. Chien, J. J. Dooley, and C. L. Davidson (2006), Potential for carbon dioxide sequestration in flood basalts, *J. Geophys. Res.*, *111*, B12201, doi:10.1029/2005JB004169.

1. Introduction

[2] A general conclusion that can be drawn from recent economic assessment models [*Edmonds et al.*, 2001; *Wigley et al.*, 1996] is that cheap and abundant fossil fuels will be a vital component of the mix of energy resources needed to sustain economic growth in both the developed and developing world [*Hoffert et al.*, 2002]. In contrast, minimizing climate change impacts from increasing atmospheric CO_2 concentrations requires dramatic reductions in CO_2 emissions from all countries if stabilization is ultimately to be accomplished [*Wigley et al.*, 1996]. Accelerating the development of near zero-emission coal-fueled power generation technology has been proposed in the United States as one means of closing the gap between the need to utilize fossil fuels while simultaneously reducing emissions [*Department of Energy* (DOE), 2003]. The technology integrates coal gasification, which can produce a relatively high-purity CO_2 stream, with geologic sequestration. Geologic sequestration involves injecting the captured CO_2 stream into a target geologic formation at depths typically >1000 m where pressure and temperature are above the critical point for CO_2 (31.6°C, 7.38 MPa) [*Bachu*, 2000].

[3] Geologic storage of carbon dioxide has been studied extensively in deep sedimentary formations because of their widespread extent and large storage capacity, typically good permeability for large-scale CO_2 injection, and extensive industry experience in oil and gas production in these formations [*Bachu and Adams*, 2003; *Intergovernmental Panel on Climate Control* (*IPCC*), 2005]. Other important geologic sequestration options include depleted oil and gas reservoirs and deep unmineable coal seams [*Brennan and Burruss*, 2003]. Site assessments for geologic sequestration of CO_2 have been conducted for the Midwest to Mid-Atlantic region of the United States [*Gupta et al.*, 2001] and at a few other locations worldwide [*IPCC*, 2005]. Sophisticated reservoir simulation of geologic sequestration is now done routinely, including coupled multiphase flow and reactive chemical transport processes [*Knauss et al.*, 2005; *Xu et al.*, 2005].

[4] Immense basalt flows exist around the world and are recognized as playing an important role in the global carbon cycle [*Brady and Gislason*, 1997; *Retallack*, 2002; *Tajika*, 1998; *Varekamp et al.*, 1992]. Large igneous provinces (LIPs) represent immense outpourings of mafic (iron- and magnesium-rich) magmas and include continental flood basalts (CFBs), volcanic passive margins, and oceanic plateaus. Shallow basaltic rocks serve as regional aquifer systems in several regions worldwide. Hence, at least some basalt formations appear to have the necessary characteristics of extent, storage capacity, and permeability to support geologic sequestration. However, a systematic and quantitative evaluation of basalts as a potential geologic storage option has not been previously developed. In this paper, a more detailed evaluation of the potential of flood basalts for permanent geologic sequestration of CO_2 is presented, making use of the extensive geological database that has been accumulated for the Columbia River basalt group in the United States, and by conducting selected laboratory experiments to better understand the chemical reactivity of

[1]Applied Geology and Geochemistry Department, Pacific Northwest National Laboratory, Richland, Washington, USA.
[2]Department of Geology, Flathead Valley Community College, Kalispell, Montana, USA.
[3]Joint Global Change Research Institute, Pacific Northwest National Laboratory, College Park, Maryland, USA.
[4]Technology Systems Analysis Department, Pacific Northwest National Laboratory, Richland, Washington, USA.

0148-0227/06/2005JB004169$09.00

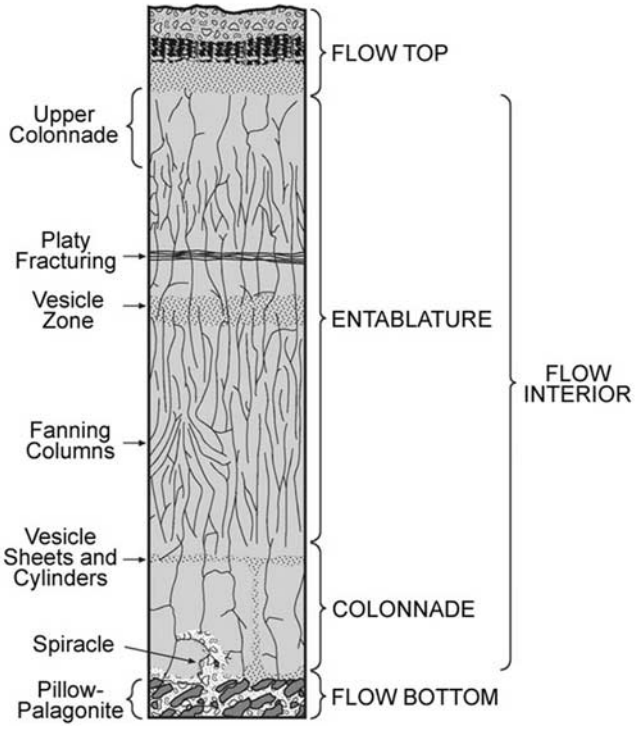

Figure 1. Major internal features of a Columbia River Basalt Group lava flow.

basalts with CO_2 charged formation water. An atlas of the major LIPs in the United States and India is also developed and compared with the existing and planned coal-fueled power station infrastructure in these countries.

2. Characteristics of Basalt Flows

[5] The internal flow features in CFB lavas are complex but certain features in the flow have potential for CO_2 sequestration. Internal features formed during the solidification of a lava flow result from variations in cooling rates, degassing, thermal contraction, and interactions with water. These features may be continuous for large distances, though their thickness is often highly variable. The uppermost section of a basalt flow (see Figure 1) consists of vesicular and brecciated basalt and is the principal feature into which CO_2 could be injected at rates exceeding a few hundred kilotons per year per well as required for sequestration of CO_2 emissions from a small to medium size coal-fueled power plant. The thickness of the vesicular portion of a flow may range from a few centimeters to almost the entire flow thickness, but most vesicular flow tops comprise 15 to 30% of the flow's thickness. Most LIPs are composed of many individual flows, tens to hundreds of layers thick.

[6] Figures 2a and 2b show thin sections of a Columbia River Basalt Group (CRBG) sample that illustrate contacts between vesicles forming interconnected pores. X-ray tomography (Figure 2c) coupled with digital image analyses of basalt flow top samples shows the pores to be mostly spheroidal and to follow a lognormal pore size distribution, in agreement with a recent study by *Shin et al.* [2005]. Total porosity of basalt flow top samples varies widely but the available pores can be highly connected, 70% and higher, at least on small-scale core samples [*Saar and Manga*, 1999; *Song et al.*, 2001].

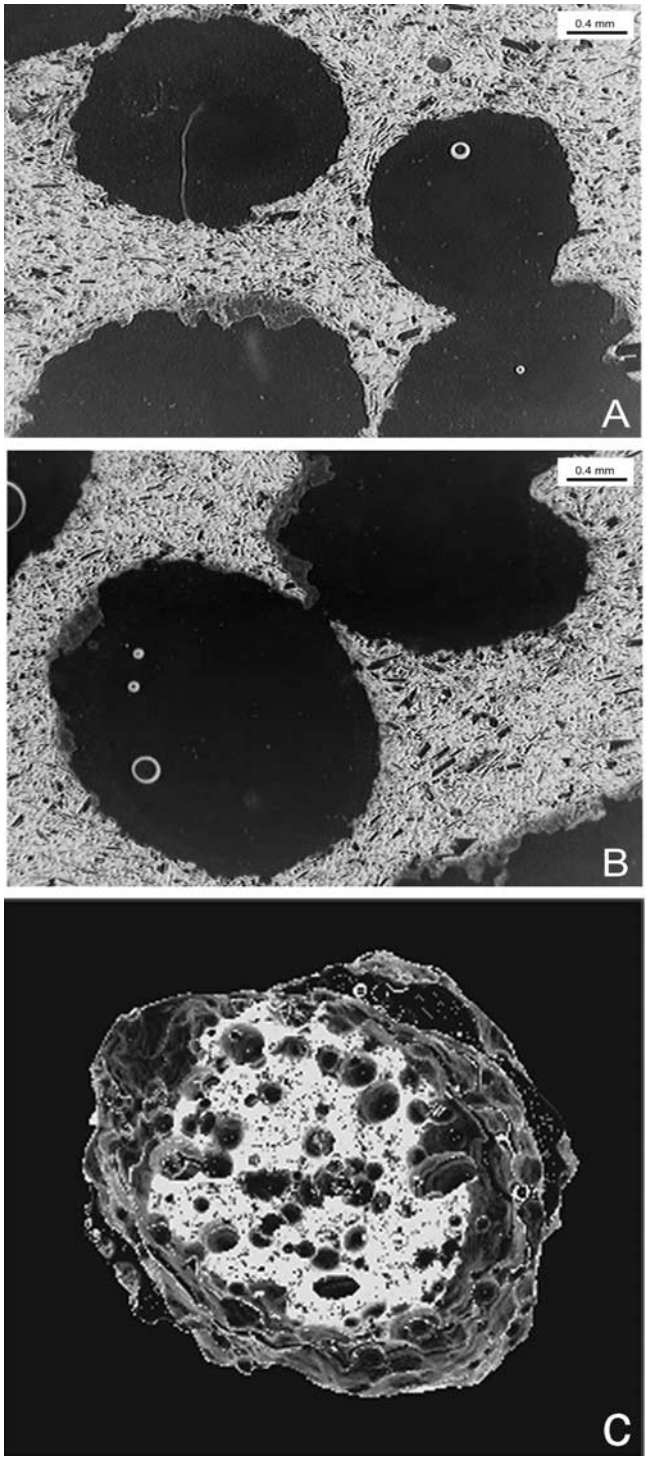

Figure 2. (a and b) Thin section of CRBG flow top taken from *Saar* [1998]. Apertures between pores can be narrow as in Figure 2a but some are wide as in Figure 2b, leading to higher permeabilities. (c) X-ray microtomograph image of Columbia River basalt flow top sample. Cut away view at the top shows distribution of vesicle sizes in the interior and how clusters of bubbles establish pore interconnectivity.

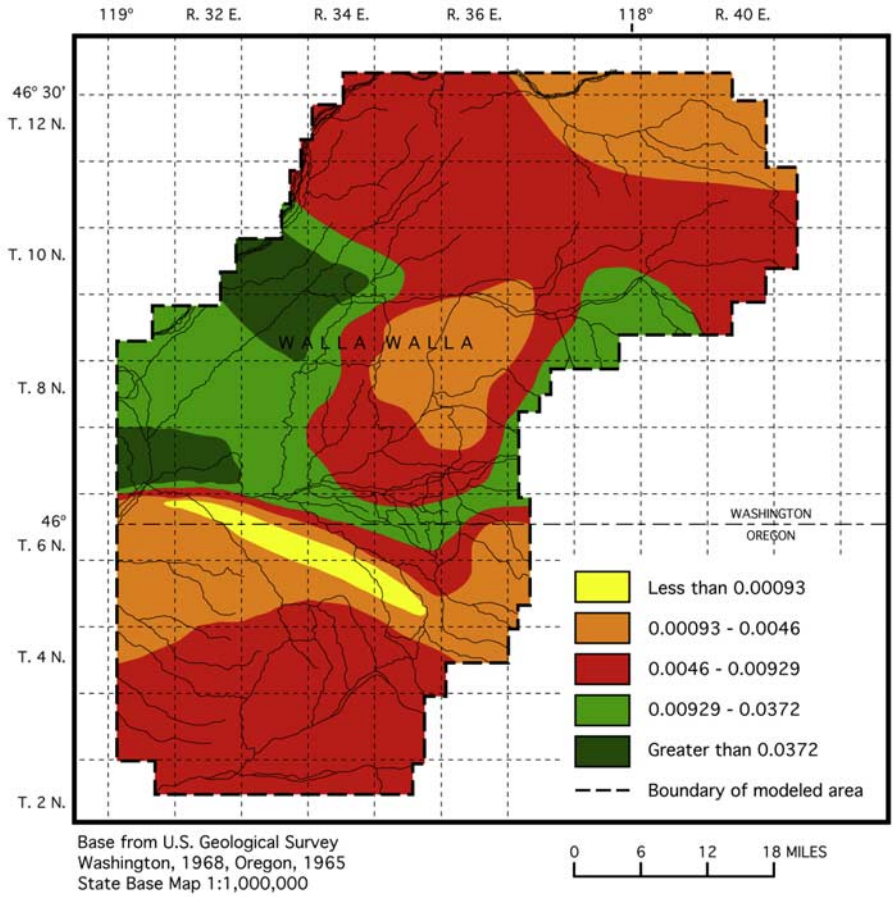

Figure 3. Transmissivity map of basalt aquifer in eastern Washington and northeastern Oregon Adapted from *MacNish and Barker* [1976]. The transmissivity values are in $m^2\ s^{-1}$.

[7] Joints are the dominant intraflow structures and form as a result of tensional stress induced from differential thermal contraction during cooling. Colonnade and entablature joints [*Tomkeieff*, 1940] form roughly vertical "columns" of rock that provide a possible pathway for CO_2 to leak to an overlying flow. However, saprolites (extensively weathered soil) and low-permeability sedimentary interbeds that occur in most basalt flows form important confining horizons. The interior of a basalt flow is also quite dense and of low permeability, potentially acting as a caprock between flows. Major chemical and isotopic differences between saline groundwaters in different CRBG flows [*DOE*, 1988] do indicate effective seals between flows (except in areas where major faulting and deformation has occurred) that would suggest limited potential for vertical migration of gas stored within deep basalt interflow zones. Multiphase flow modeling of CO_2 injection into fractured CRB shows only 50 m vertical movement above the injection horizon 17 years post injection [*White and McGrail*, 2005]. However, field pilot studies will be required to validate these numerical simulations, which can only approximate the complex fracture network in a real basalt formation.

3. Large-Scale Permeability and Connectivity

[8] Upscaling core-scale properties of vesicular basalts to kilometer-scale regions of importance for CO_2 sequestration presents numerous challenges, especially because of the inherent heterogeneous nature of flood basalts. Nevertheless, evidence of lateral continuity can be found where basalts serve as regional aquifer systems. The occurrence and transfer of groundwater through a basalt aquifer is controlled by several factors including tectonic activity, topographic features, structural dislocations, and erosional processes. These factors and others dictate the lateral continuity, thickness, and composition of the individual lava flows. Examples of basalt aquifers in North America include Carson River Basin in Nevada [*Lico and Seiler*, 1994], the Modoc Plateau and the Cascade Mountains in northern California [*U.S. Geological Survey* (*USGS*), 1999], Snake River Plane Aquifer in Idaho [*Bishop et al.*, 2004], northern New Mexico [*Wels et al.*, 2000], and the CRBG in

eastern Washington and Oregon [*MacNish and Barker*, 1976]. Examples of basalt aquifers from other parts of the world include the Hawaiian Islands [*USGS*, 1999] and the Deccan basalts in western India [*Kulkarni et al.*, 2000].

[9] The CRBG contains several regional aquifer systems serving eastern Washington and northeastern Oregon that consist of a layered series of highly conductive aquifer zones alternating with dense basalt zones of very low hydraulic conductivity [*Luzier and Burt*, 1974]. Wells have penetrated the thick sequence of basalt flow tops to meet irrigation, industrial, and public water supply needs since the early 1900s. Typically, wells drilled into the basalt are uncased and penetrate several aquifer zones. Drilling records and borehole geophysical logs show downhole flows from one aquifer zone to another. According to some reports, cascading groundwater can be heard in the wellbore as the water moves from a higher zone to an isolated lower zone [*Luzier and Burt*, 1974].

[10] The Walla Walla Watershed Plan (*Walla Walla Watershed Planning*, 2005, available at http://www.wallawallawatershed.org/wplan.html#One) describes the CRBG aquifer system as being heterogeneous and water transmission is achieved through vesicular and scoriceous interflow zones. *MacNish and Barker* [1976] measured the relative ability of these aquifers to transmit groundwater. Data from aquifer tests conducted on more than 100 wells drilled into the CRBG were used to establish a regional transmissivity map of eastern Washington and northeastern Oregon (Figure 3), near the small community of Walla Walla [*MacNish and Barker*, 1976]. Generally, transmissivity values for the flow top basalt are highest ($>0.0372\ m^2\ s^{-1}$) in areas that are relatively flat and undisturbed in the western and northwestern parts of the basin (Figure 3). In the southwest section of the map, very low transmissivity values ($<0.00093\ m^2\ s^{-1}$) correspond to an area that experienced uplift after emplacement of the basalt. Obviously, the effects of structural displacement can alter transmissivity of a basalt flow dramatically.

[11] Total water storage capacity of the basalt aquifer as reported by *Hanson and Mitchell* [1977] was over $3 \times 10^9\ m^3$. Estimated annual recharge rate of the basalt aquifer system is reported to be $1.6 \times 10^8\ m^3\ yr^{-1}$ [*MacNish and Barker*, 1976]. These examples from shallow basalt aquifer systems are important because deeper basalts that are the potential targets for CO_2 sequestration are expected to have similar large-scale transmissivity and capacity values. Shallow basalt aquifer systems are not potential or viable injection targets. Deep basalts contain brackish formation water that is not suitable for drinking water or irrigation purposes. Estimates of the potential CO_2 storage capacity in the CRBG are provided in section 6.

4. In Situ Mineralization

[12] Deep sedimentary rock formations are considered the leading option for CO_2 sequestration because of their huge estimated capacity for CO_2 storage and widespread geological occurrence [*Bachu*, 2000]. However, there is insufficient Ca, Mg, and Fe in the rocks that make up a typical sedimentary formation to support significant mineral trapping [*Johnson et al.*, 2004; *Sass et al.*, 2001], a chemical process where injected CO_2 is converted to stable carbonate minerals. Consequently, the injected CO_2 will be stored for long times as a supercritical fluid [*Pruess and García*, 2002] that will mix very slowly with the formation brine [*Lindeberg and Wessel-Berg*, 1997] and so may be subject to slow leakage processes [*Dooley and Wise*, 2003]. Table 1 shows a typical bulk chemical composition for Columbia River and Deccan basalts from western India. Crystalline components for the basalt samples were identified by X-ray diffraction. Plagioclase feldspars and pyroxenes are the major crystalline components in these basalts. Minor amounts of quartz and olivine were also identified. Secondary mineral phases such as carbonates, clays, and zeolites were detected in the more weathered Deccan sample. Overall, the basalt samples appeared very similar in mineralogy with only minor differences observed in the secondary phases.

Table 1. Average Chemical Composition of Basalt Samples Representing Columbia River and Deccan Basalts[a]

Component, wt%	CRB	Deccan
Na_2O	2.79	2.62
MgO	5.16	5.03
Al_2O_3	15.0	12.9
SiO_2	51.1	50.7
P_2O_5	0.46	0.39
K_2O	0.44	0.66
CaO	8.84	9.79
TiO_2	2.11	3.39
MnO	0.17	0.22
FeO	13.3	14.3

[a]Chemical analyses were performed by X-ray fluorescence spectroscopy. The CRB sample is a flow top sample from the Grande Ronde basalt formation obtained from core hole DC-6 located on the Hanford site in Washington State. The Deccan basalt was obtained from basalt outcrops in western India and was supplied by Washington State University.

[13] As Table 1 suggests, these basalts contain up to 25% combined molar concentration of Ca, Fe, and Mg in crystalline silicates and glassy mesostasis. These cations form solid carbonates with dissolved CO_2 under the proper conditions. In situ mineral carbonation is attractive because (1) no additional energy input (other than for injection), mining, or waste disposal is required as compared with proposed ex situ mineralization processes [*Lackner et al.*, 1997; *O'Connor et al.*, 2002] and (2) injected CO_2 is permanently stabilized and not subject to leakage.

[14] A general mineralization reaction scheme for plagioclase group minerals is

$$CO_2(g) \overset{K_h}{\rightleftharpoons} CO_2(aq) \tag{1}$$

$$\downarrow$$

$$CO_2(aq) + H_2O \overset{K_1}{\rightleftharpoons} HCO_3^- + H^+ \tag{2}$$

$$\downarrow$$

$$Na_x(Ca, Mg, Fe)_y Si_3AlO_8 + (x + 2y + 3)H^+ + 4H_2O \xrightarrow{k_2} xNa^+ + y(Ca, Mg, Fe)^{2+} + 3H_4SiO_4(aq) + Al^{3+} \tag{3}$$

$$\downarrow$$

$$(Ca, Mg, Fe)^{2+} + HCO_3^- \overset{K_3}{\rightleftharpoons} (Ca, Mg, Fe)CO_3 + H^+ \tag{4}$$

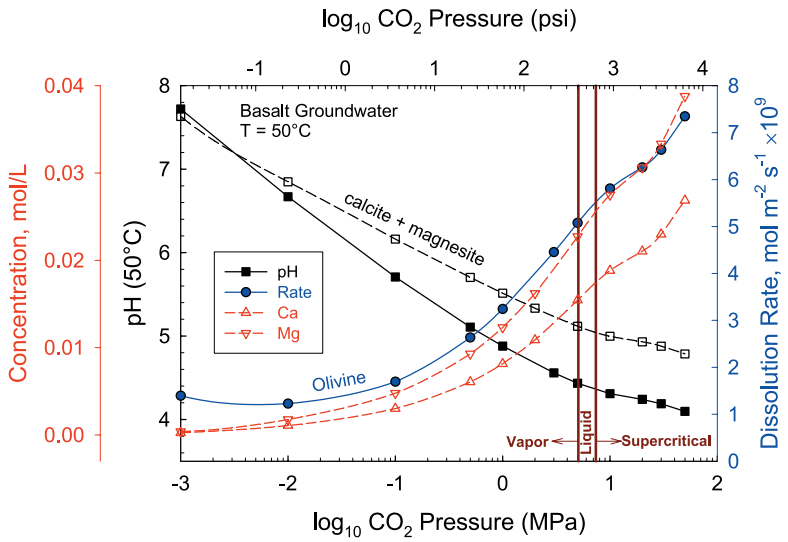

Figure 4. Calculated change in solution pH of typical CRBG basalt groundwater as a function of CO_2 pressure and its effect on aqueous dissolution rate of olivine. Dashed lines represent computed values assuming equilibrium with calcite and magnesite is eventually established.

where K_h is Henry's constant, K_1 and K_3 are equilibrium constants, and k_2 is a kinetic rate constant. Pressurization with CO_2(g) causes production of carbonic acid [CO_2(aq)], bicarbonate anions, and H^+ via reactions (1) and (2), respectively, thus reducing the solution pH.

[15] For a typical basalt groundwater composition [*Reidel et al.*, 2002], the calculated change in pH with increasing CO_2 pressure is given in Figure 4. The calculations were performed with the EQ3NR geochemical code [*Wolery*, 1992]. In conducting these calculations, corrections were made to K_h to account for pressure, temperature, fugacity, and ionic strength effects in the basalt groundwater at high CO_2 pressure [*Pruess and García*, 2002]. Olivine, pyroxene, and plagioclase that are saturated or slightly supersaturated at low CO_2 pressure are many orders of magnitude undersaturated at supercritical CO_2 pressures and so will dissolve according to an irreversible dissolution reaction such as (3). Using an activation energy of 79.5 kJ mol^{-1} [*Wogelius and Walther*, 1992] and pH-dependent dissolution rate equation [*Wogelius and Walther*, 1991], the calculated dissolution rate of olivine at 50°C as a function of CO_2 pressure is given in Figure 4. The mechanism of dissolution of olivine group minerals in acidic solutions appears to be a fast ion exchange reaction of H^+ with the divalent metal cations followed by a much slower rate-controlling step involving proton absorption on silica dimmers [*Pokrovsky and Schott*, 2000]. The mechanism is consistent with experimental data that shows a 0.5 order dependence of the dissolution rate on H^+ activity under acidic conditions [*Pokrovsky and Schott*, 2000; *Westrich et al.*, 1993; *Wogelius and Walther*, 1991]. Still, the dissolution rate for the primary phases in basalt is many orders of magnitude slower than precipitation kinetics for calcite via reaction (4) [*Zhang and Dawe*, 2000]. Irreversible dissolution reactions such as (3) could determine how fast carbonate mineralization will occur in basalt formations, depending on availability (transport) of CO_2 to support the reactions. We will discuss this in more detail later.

[16] Dissolution of the basalt minerals also causes the solution pH to rise until carbonate precipitation begins. Figure 4 (dashed lines) shows the calculated solution pH and the Ca and Mg concentrations in equilibrium with calcite ($CaCO_3$) and magnesite ($MgCO_3$) as a function of CO_2 pressure. The data in Figure 4 show that relative predominance of Ca versus Mg in the basalt determines which carbonate mineral precipitates with the more calcic basalts favoring formation of calcite because of its lower solubility.

[17] Laboratory experiments with CRBG samples exposed to water and supercritical CO_2 validate the basic hypothesis of carbonate mineralization with basalts. Figure 5a shows massive mineral carbonation on a basalt grain exposed to CO_2-saturated water for 32 weeks. X-ray diffraction and Raman spectroscopic measurements conclusively identify the precipitate as calcite. However, longer term experiments conducted over one year or more show a phase transition to ankerite ($Ca(Fe,Mg)(CO_3)_2$), which is consistent with observations in some natural CO_2-charged reservoirs [*Franks and Forester*, 1984; *Gouze and Coudrain-Ribstein*, 2002] and geochemical simulations [*Xu et al.*, 2004]. Scanning electron microscope images obtained from cross sections of reacted grains (Figure 5b) show sharp interfaces with less reactive phases such as pyroxene protruding into the calcite. A possible interpretation is that the more reactive surrounding glassy mesostasis has dissolved leaving the pyroxene crystal exposed at the surface, which then became covered with precipitating calcite. Elemental mapping by wavelength dispersive X-ray spectroscopy shows the calcite also contains Mg, Fe, S, and Mn. The cation substitution is an early indicator of the phase transition to ankerite detected in longer-term experiments. The phase transition is expected to occur as a natural paragenetic sequence but may also be assisted from depletion of the glass phase on the surface of the basalt grains allowing the more durable crystalline phases (pyroxene, plagioclase) to begin to dominate the solution chemistry.

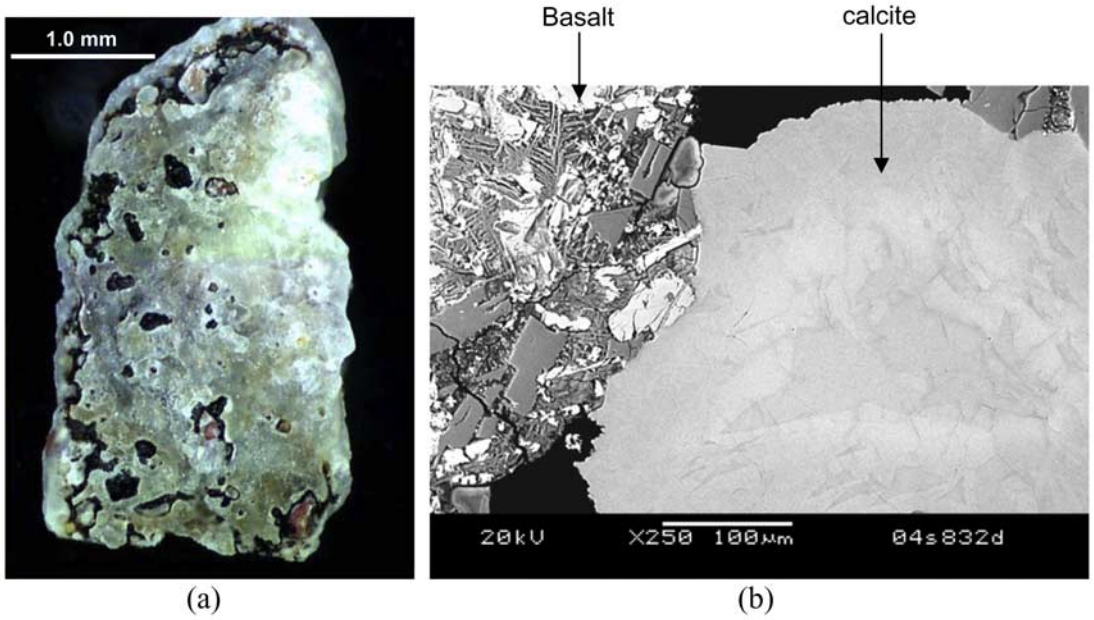

Figure 5. (a) Optical photo of grain of Rocky Coulee basalt flow top from Washington State after 32 weeks of exposure to deionized water and CO_2 at 10.3 MPa and 90°C. Note how nearly the entire grain surface is coated with calcite. (b) SEM micrograph of basalt grains removed from the same test. Light areas of the basalt grains are pyroxene and the darker regions are plagioclase feldspar and glassy mesostasis. The precipitate on the right was identified by XRD as calcite. However, wavelength dispersive X-ray spectroscopy shows that the precipitate contains minor substitutions of Mg, Fe, S, and Mn. The slightly darker zones were enriched with Mg and S, whereas the lighter zones had higher Fe and Mn content.

[18] Although most basalts contain significantly more iron than either calcium or magnesium combined, we have not detected siderite ($FeCO_3$) as a reaction product. Siderite has much slower precipitation kinetics than calcite [*Greenberg and Tomson*, 1992; *Jensen et al.*, 2002]; years may be required before significant siderite precipitation is likely to be detected in these laboratory experiments.

5. Estimation of In Situ Mineralization Rate

[19] Computation of the rate of carbonate mineral formation in a real basalt formation requires detailed information on the following three items at a minimum: (1) solution concentrations of Ca, Mg, Fe, and Mn required to precipitate calcite or other carbonates, (2) release rate of Ca, Mg, Fe, and Mn from the basalt, and (3) concentration of dissolved CO_2. Solution concentrations required to precipitate calcite (assuming only minor substitution of Mg, Mn, and Fe) can be calculated from geochemical modeling, as illustrated in Figure 4. The release rate of Ca and other metal cations from basalt is a function of temperature, pH, and the surface area of the basalt. The concentration of dissolved CO_2 is a function of time and space in the reservoir and must be evaluated through reservoir simulation. Because pH is a function of the dissolved CO_2 concentration, and calcite solubility and basalt dissolution are strong functions of pH, 1, 2, and 3 are strongly coupled. Hence rigorous calculation of carbonate mineralization rates requires solving a complex reactive chemical transport problem. Our research group is presently conducting such calculations but simpler approximations are introduced here to provide a bounding estimate of carbonate mineralization rate.

5.1. Calcite Solubility

[20] When CO_2 is introduced into the reservoir, the ambient chemical conditions of the pore water are significantly perturbed from their initial state. To compute the Ca concentration required to precipitate calcite, we ignore rates of CO_2 mixing into the vesicular pores of the basalt and simply assume that the vesicles are filled with formation water in equilibrium with CO_2 at the prevailing hydrostatic pressure and temperature as a function of depth. With this assumption, and compiling ranges of groundwater compositions determined as a function depth in the CRBG, the amount of Ca that must be dissolved from the basalt to initiate calcite precipitation was calculated and is shown in Figure 6.

5.2. Release Rate From Basalt

[21] Next, to compute rates of Ca release from basalt, we utilize dissolution kinetics data collected in our laboratory on representative CRBG samples. Details on the experiments are described in a separate publication (H. T. Schaef and B. P. McGrail, Dissolution kinetics of Columbia River Basalt under mildly acidic conditions relevant to geological sequestration of carbon dioxide, submitted to *Applied Geochemistry*, 2006). The key results of importance to this study are shown in Figure 7. We fit these data to a kinetic rate law

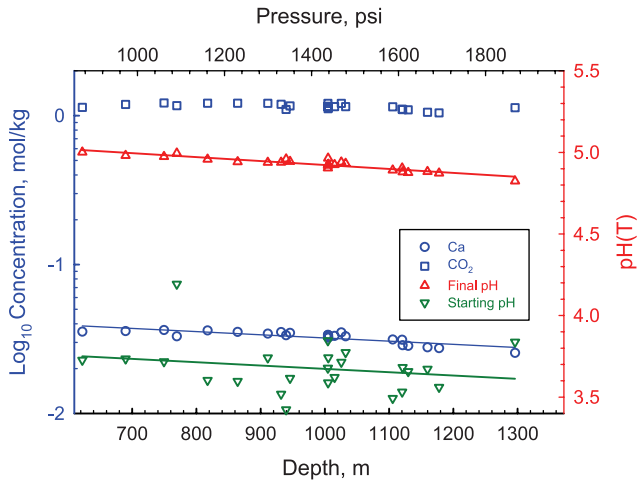

Figure 6. Calculated solution composition as a function of depth in typical CRBG basalt groundwater. Inverted triangle indicates calculated starting pH of fluid samples taken from core hole DC-6 [*Early et al.*, 1986] brought to equilibrium with CO_2 at local hydrostatic pressure. Red triangle, blue circle, blue square indicate final pH, CO_2, and Ca concentrations calculated from starting fluid compositions assuming equilibrium with calcite and CO_2 at local hydrostatic pressure.

developed for silicate minerals [*Aagaard and Helgeson*, 1982] of the form

$$r_d = k_o 10^{\eta[\mathrm{pH}]} \exp\left(-\frac{E_a}{RT}\right) \tag{5}$$

where r_d is the normalized release rate (g m^{-2} d^{-1}), k_o is the intrinsic rate constant (g m^{-2} d^{-1}), η is the pH power law coefficient, E_a is the activation energy (kJ mol^{-1}), R is the gas constant (kJ mol^{-1} K^{-1}), and T is the temperature (K). The regressed parameters are $k_o = 1.7 \times 10^4 \pm 1.9 \times 10^4$ g m^{-1} d^{-1}, $\eta = -0.18 \pm 0.02$, and $E_a = 26.0 \pm 3.2$ kJ mol^{-1}. Because temperature is a known function of depth, and pH has been computed previously (Figure 6), equation (5) can be used to compute the rate of Ca release as function of depth in the basalt formation. However, the rate equation only provides the mass flux of Ca per unit surface area. The surface area of the basalt associated with the vesicles must be calculated to compute the total mass flux.

5.3. Basalt Vesicle Surface Area

[22] The vesicle size distribution in basalts can be described by statistical functions [*Sahagian et al.*, 1989; *Sahagian and Maus*, 1994]. Because vesicular surface area has been correlated with a lognormal distribution [*Shin et al.*, 2005], we will use this form of probability distribution function to represent bubble size distribution, and neglect eccentricity in the vesicles by assuming all are perfect spheres. The probability distribution is then given by

$$p_p(x) = \frac{\exp\left(-\frac{[\ln(x)-x_o]^2}{2b^2}\right)}{bx\sqrt{2\pi}} \tag{6}$$

where x is the vesicle diameter, x_o is the mean vesicle diameter, and b is the distribution shape parameter. Staying in spherical geometry, the total pore volume in a volume V of vesicular basalt of radius r, where $r \gg x_o$, is then given by

$$\varepsilon V = n\int_0^\infty V_p(x)p_p(x)\,dx = n\int_0^\infty \cdot\frac{4}{3}\pi(x/2)^3\frac{\exp\left(-\frac{[\ln(x)-x_o]^2}{2b^2}\right)}{bx\sqrt{2\pi}}dx \tag{7}$$

where ε is the total porosity, n is the total number of pores (vesicles), V_p is the volume of each pore with average diameter x. The total surface area associated with the vesicles (A_p) is then given by

$$A_p = n\int_0^\infty \pi x^2 p_p(x)\,dx \tag{8}$$

The value of principal interest is the surface area of the basalt in the vesicles normalized to the total vesicle volume (S_r) and is given by

$$S_r = \frac{A_p}{V_p} = \frac{6\int_0^\infty x^2 p_p(x)\,dx}{\int_0^\infty x^3 p_p(x)\,dx} = 6\exp\left[-\left(x_o + \frac{5b^2}{2}\right)\right] \tag{9}$$

An important consequence arising from equation (9) is that reactive surface area to volume decreases exponentially with the mean vesicle diameter. Hence knowledge of the vesicle size distribution in the target formation is a critical parameter in our analysis.

5.4. Calcite Precipitation Induction Time

[23] Figure 8 shows the range of measured groundwater compositions, temperature, and pH as a function of depth in Grande Ronde basalt [*Early et al.*, 1986]. Both the Ca and Mg concentrations vary little with depth, hence the initial Ca concentration can be assigned a constant value $C_o \approx 2$

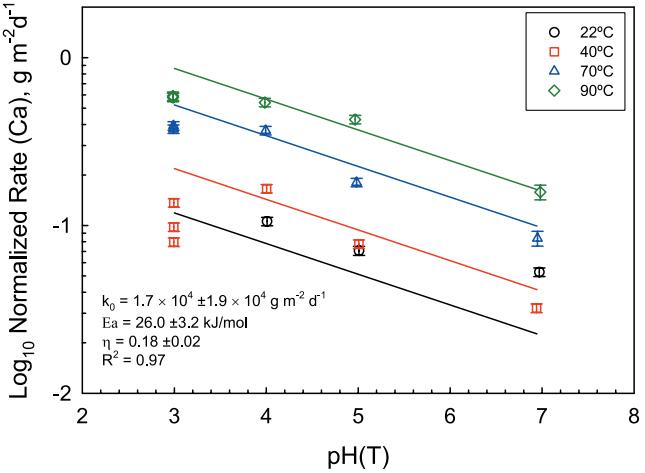

Figure 7. Dissolution rate of Columbia River basalt as a function of pH and temperature. Solid lines represent results from a nonlinear fit of the data to equation (5).

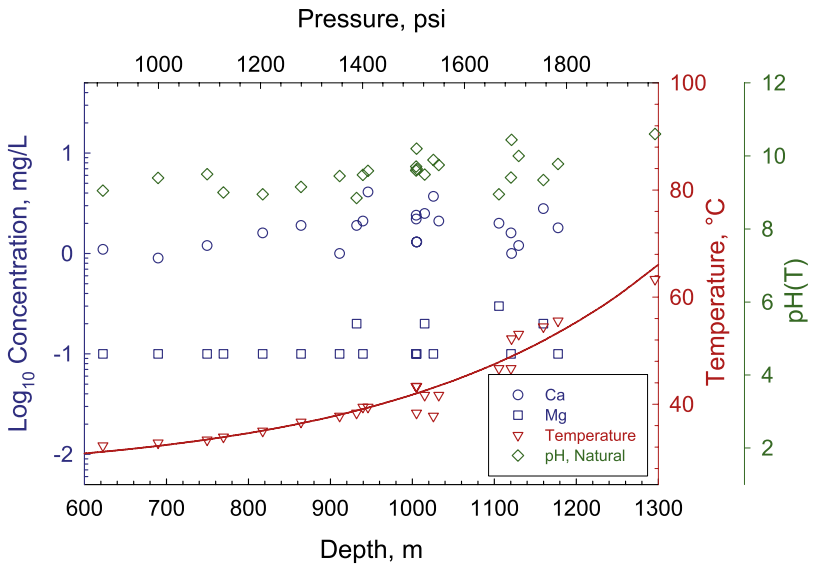

Figure 8. Initial chemical composition of Grande Ronde basalt groundwater and temperature profile with depth [*Early et al.*, 1986]. The line was calculated from a nonlinear regression fit to equation (10).

mg L^{-1}. The temperature data were fit to an exponential function of the form

$$T(d) = T_o + ae^{bd}. \tag{10}$$

where $T(d)$ is the temperature as function of the depth d, T_o, a, and b are fitting parameters. We find for the regressed parameters $T_o = 26.5 \pm 3.1°C$, $a = 0.63 \pm 0.5°C$, $b = 0.0032 \pm 0.0006$ m^{-1}.

[24] To compute the induction time for calcite precipitation at any given depth, a solution is needed to the nonlinear mass balance equation for the Ca concentration C

$$V_p \frac{dC}{dt} = A_p f_{Ca} r_d[\mathrm{pH(C)}, T] \tag{11}$$

subject to the initial condition $C[0] = C_o$ and where f_{Ca} is the mass fraction of Ca in the basalt. Equation (11) is nonlinear because the pH is increasing as a function of the Ca concentration (because of basalt dissolution) until the equilibrium concentration with respect to calcite is reached. To make analytical solutions possible, we assume a simple linear-dependent change in pH as a function of Ca concentration given by

$$\mathrm{pH}(C) = \mathrm{pH_o} + \frac{\mathrm{pH_f} - \mathrm{pH_o}}{C_s - C_o}(C - C_o) \tag{12}$$

where pH_o is the pH of the initial pore water in equilibrium with CO_2 at the local hydrostatic pressure, pH_f is the pH in equilibrium with calcite, C_s is the calculated Ca concentration in equilibrium with calcite. Substituting (5) and (12) into (11) and solving for $C(t) = C_s$, the induction time t_p is

$$t_p = \frac{(C_s - C_o)(10^{\eta \mathrm{pH_f}} - 10^{\eta \mathrm{pH_o}})10^{-\eta(\mathrm{pH_f} + \mathrm{pH_o})}}{f_{Ca} k_o \eta (\mathrm{pH_f} - \mathrm{pH_o}) \exp\left(\frac{-E_a}{RT}\right)} \frac{V_p}{A_p} \tag{13}$$

[25] All the parameters needed to compute t_p have been given in the previous sections, with the exception of the ratio V_p/A_p $(1/S_r)$. This requires a detailed geological characterization of the vesicle size distribution in the basalt horizons to be used for injection. To obtain an estimate of the V_p/A_p ratio, we fit our lognormal distribution to the data given by *Sahagian and Maus* [1994] for a Hawaiian basalt. The data giving reasonable fits to the reported distribution are $x_o = 1.46 \pm 0.017$ mm, and 1.48 ± 0.073 mm, and $b = 0.19 \pm 0.01$, and 0.34 ± 0.06, respectively. Putting these values into equation (9) gives $S_r = 1273$ and 1023 m^{-1}, respectively. These values can be compared against the data of *Saar* [1998] shown in Figure 9 for CRBG samples obtained from central and eastern Oregon. For the important range in basalt samples with connected porosity between 10 and 40%, the vesicular surface area-to-volume ratio ranges between 500 and 1300 m^{-1}. These values are within the

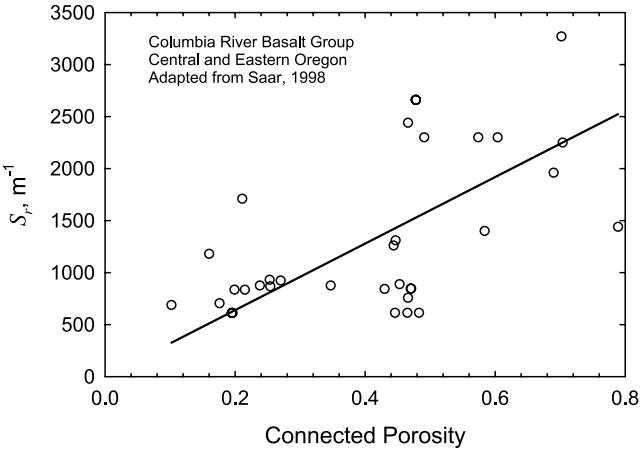

Figure 9. Specific surface area of CRBG samples obtained from central and eastern Oregon. Adapted from data given by *Saar* [1998].

Table 2. Input Data Used to Compute Induction Time for Calcite Precipitation in Grande Ronde Basalt Formation

Depth, m	T, °C	pH_o	pH_f	r_d, g m^{-2} d^{-1}	C_s, g m^{-3}	t_p, days
800	35	3.72	4.97	2.9×10^{-3}	1419	964
900	38	3.70	4.95	3.3×10^{-3}	1351	822
1000	42	3.68	4.92	3.8×10^{-3}	1286	678
1100	48	3.65	4.90	4.6×10^{-3}	1225	534
1200	56	3.63	4.87	5.9×10^{-3}	1166	397
1300	67	3.61	4.85	8.1×10^{-3}	1110	275

range estimated by our statistical model (9) using the bubble size distribution data given by *Sahagian and Maus* [1994].

[26] Taking a minimum S_r value of 500 m^{-1} and putting in all the remaining parameters into equation (13), values for t_p were calculated and are provided in Table 2. The calculations indicate that the time required to begin precipitating calcite is relatively short, on the order of 1.5 yr for a target depth of 1100 m. However, the key implicit assumption in this estimate is that equilibrium with CO_2 has been established with the formation pore water. In practice, time will be required for dissolution and dispersion of the CO_2 into the formation pore water [*Lindeberg and Wessel-Berg*, 1997]. Hence the key question is whether the rate of carbonate mineral precipitation is controlled by the rate of supply of cations (Ca^{2+}, Mg^{2+}, Fe^{2+}) from basalt dissolution or by dispersion of dissolved CO_2.

[27] It is possible to answer this question semiquantitatively by computing the Damköhler number (*Da*) for the basalt-water-CO_2 system. The Damköhler number is a ratio of the rate of chemical reaction versus mass transport. The calculation can be performed with a starting assumption of CO_2-saturated pore water in a fixed volume of basalt. We take the numerator for the chemical reaction term to be simply $S_r \times f_{Ca} \times r_d$ or the volumetric rate of Ca release from the basalt into the CO_2-saturated water. Because we have assumed equilibrium with CO_2, the molar rate of Ca supply from basalt dissolution is then exactly equal to the molar rate of CO_2 consumption from calcite precipitation.

[28] For the mass transport term in the denominator, the fastest rate would occur via convection associated with Rayleigh-Taylor instabilities [*Lindeberg and Wessel-Berg*, 1997]. Rayleigh-Taylor instabilities occur when a more dense fluid overlies a less dense phase in the presence of an orthogonal gravitational field. They produce fingering flow patterns and are very sensitive to porosity, permeability, and pore size [*De Wit*, 2004; *Wilke*, 1995]. Because CO_2-saturated pore water is slightly more dense (≈1%) than the initial in situ pore water, Rayleigh-Taylor instabilities are likely to accelerate CO_2 mixing in vesicular basalts, perhaps by several orders of magnitude, relative to diffusion alone. For the present analysis, we consider a cubic volume of basalt with edge length l and further conservatively assume fingering convection occurs across the entire cross section of the volume. The velocity of the finger flow through this volume (U) is given by [*De Wit*, 2004; *McGrail et al.*, 2003]

$$U = \frac{\beta(\rho_s - \rho_o)gK}{\varepsilon\nu} \tag{14}$$

where β is a coefficient specific to the porous medium, ρ_s is the CO_2-saturated fluid density, ρ_o is the initial pore fluid density, g is the gravitational acceleration constant, K is the permeability of the porous medium, and ν is the viscosity. Then, *Da* is given by

$$Da = \frac{S_r f_{Ca} r_d}{\frac{\beta(\rho_s - \rho_o)gK}{\nu l} C_s}. \tag{15}$$

[29] For a target injection depth of 1000 m, the temperature from Figure 8 is ~40°C; from Figure 6, the pH in equilibrium with calcite is ≈5, and the dissolved CO_2 concentration is C_s = 1.1 mol kg^{-1}. From Figure 8, $r_d \approx$ 0.1 g m^{-2} d^{-1} at pH 5 and 40°C. Although a value for β is unknown for vesicular basalt, we will assign β = 0.5 as a reasonable value for an equivalent porous medium [*Kerr and Tait*, 1985]. The initial water density is ρ_o = 996 kg m^{-3} and for the CO_2-saturated pore water we assign ρ_s = 1007 kg m^{-3}. Viscosity is taken the same as pure water at 40°C, $\nu = 6.54 \times 10^{-4}$ Pa s [*Lemmon et al.*, 2005]. Taking l = 1 m, and S_r = 500 m^{-1} as determined previously, all the parameters in equation (15) have been estimated, with the exception of the permeability (K). By setting Da = 1 in equation (15), the permeability where the crossover occurs between chemical reaction control and mass transport control is ~10^{-16} m^2 (0.1 mdarcy). Hence, for this example problem, dispersion of the CO_2 by buoyancy-aided convection occurs much faster that its consumption by carbonate precipitation except in very low permeability basalts.

[30] The perturbation theory used to analyze Rayleigh-Taylor instabilities in porous media requires that wavelength of the perturbations be significantly larger than the dimensions of the pores propagating the perturbations. It is easy to show that this is true for a typical sandstone but mean vesicle size in basalts is typically far bigger than in sandstone reservoirs. Hence the validity of the hypotheses used to assess hydrodynamic mixing of supercritical CO_2 and water needs to be reexamined for basalt rock systems. Also, we have assumed a constant rate of Ca supply from dissolution of the basalt. This may not be true because surface coatings of calcite and other alteration products may slow the dissolution kinetics. Our laboratory test data do not indicate a diminution of Ca release rate with time but the test durations are still too short to draw any definitive conclusions about surface armoring effects. Even if armoring reactions slowed Ca release significantly, the unreacted CO_2 would then continue to spread, dissolve into vesicle pore water, and thereby contact fresh surface for the dissolution and precipitation reactions to proceed.

6. Discussion

[31] On the basis of the available information discussed in the previous section, basalt formations do have the necessary characteristics to be considered as an option for geologic sequestration of carbon dioxide. In the following sections, we consider their storage potential in more detail in both the United States and India.

6.1. Basalt Sequestration Options in the United States

[32] There are major basalt flows in four regions of the United States (see Figure 10) that might be attractive targets

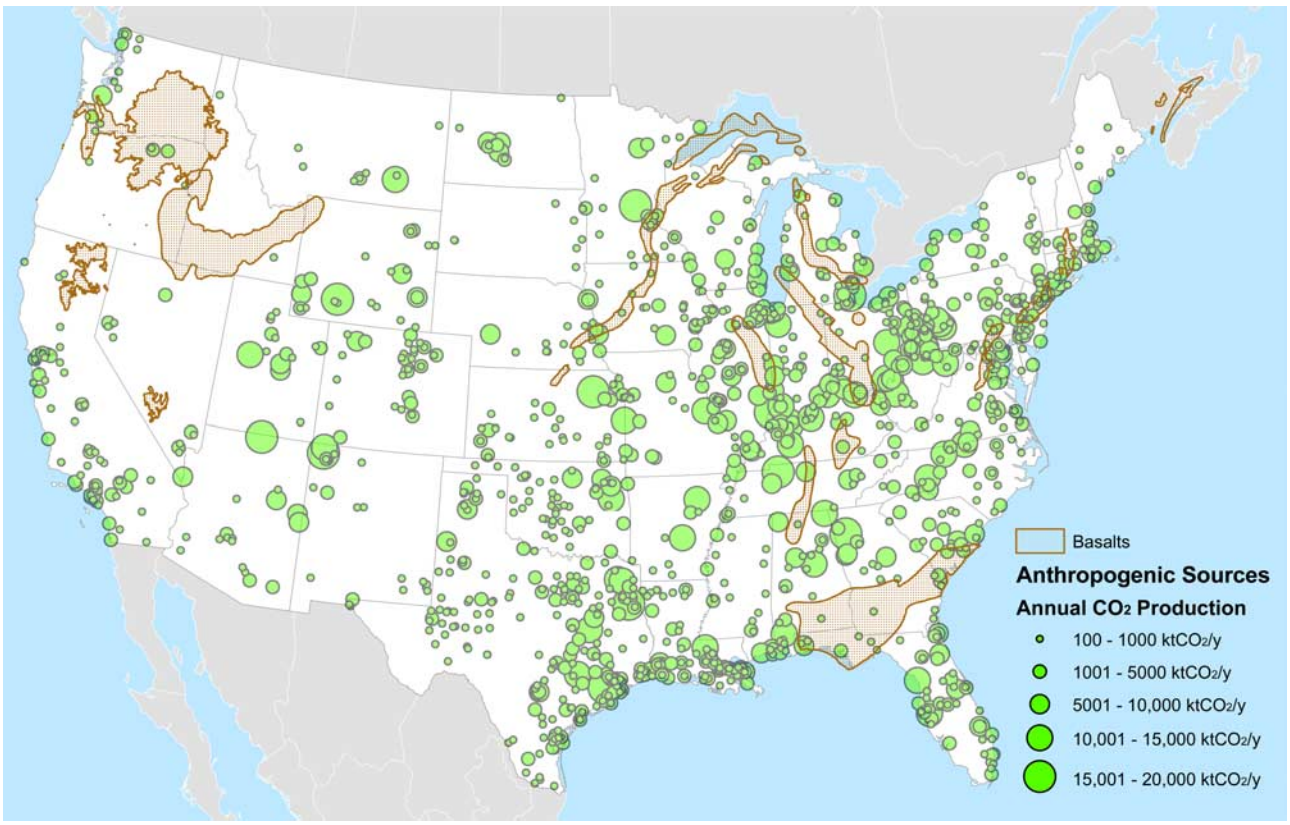

Figure 10. Distribution of major basalt formations in the United States along with distribution of CO_2 sources.

for CO_2 sequestration. Along the eastern margin of North America, the Newark Supergroup contains sediments and volcanic rocks preserved in these rift basins. Tholeiitic lava flows (rich in aluminum and low in potassium) are found only in the northern and western parts of these basins. Of the basins containing basalt, the Newark and Hartford basins are the largest and most studied. Both basins contain three basalt sections separated by sediments and a deep, genetically related sill [*Seidemann et al.*, 1984]. The Watchung Basalts in the upper Midwest are interbedded with 170–500 m of sediments [*Puffer et al.*, 1981]. Individual flow thicknesses are up to 100 m (Holyoke basalt in the Hartford basin); the thickest of the Watchung flows is the Preakness flow (up to 180 m thick) [*Puffer and Volkert*, 2001]. This group of basalts is also located near a significant concentration of CO_2 emission sources, primarily fossil fuel power plants (Figure 10).

[33] The Central Atlantic Mafic Province (CAMP) is an early Mesozoic province related to the opening of the Atlantic Ocean that extends in the United States from the northeast along the Appalachians to the Gulf of Mexico. The South Georgia Rift is a complex terrane of rift basins with subbasins up to 100 km wide and over 7 km deep. The basins are filled with sediments and volcanics. Like the Newark basin, the fill is typically about 6 km thick as interpreted from seismic reflection lines. Much is sediment, but mafic igneous rocks are also present [*McBride*, 1991]. Although little is known about the structure and extent of this flow, the region does intersect a concentrated area of CO_2 emission sources from power plants (Figure 10).

[34] The CRBG, which is part of the larger Columbia Plateau Province shown in Figure 10, is probably the most well-studied LIP in the world, despite its small size relative to other known CFBs. There are over 300 lava flows that comprise CRBG; it covers more than 164,000 km^2 of Washington, Oregon, and Idaho with a total volume of over 174,000 km^3. Each flow is from a few tens of meters to 100 m thick. The U.S. Department of Energy spent over $400M in numerous studies of the basalts and the basalt aquifer systems for nuclear waste remediation at the Hanford Site and for natural gas storage [*Reidel et al.*, 2002]; a very large body of information is available to provide an estimate of the CO_2 storage capacity in the CRBG. Assuming an interflow thickness of 10 m with an average porosity of 15% and 10 available interflow zones at an average hydrostatic pressure of 100 atm, the storage potential is greater than 100 Gt CO_2. This capacity is more than sufficient to sequester the entire emissions of the northwestern United States for the foreseeable future. The CRBG is also situated in an area of seismic stability, several hundred kilometers east of the North American Plate margin. Seismicity is characterized mainly by sparse, magnitude 1–2 earthquakes that typically occur randomly throughout the province. This seismic activity has had no effect on aquifer isolation as demonstrated by laterally continuous and isotopically distinct aquifer systems [*Reidel et al.*, 2002].

6.2. Geologic Sequestration Options in India

[35] Several massive basalt flows occur around the world [*Eldholm and Coffin*, 2000; *Huang and Opdyke*, 1998;

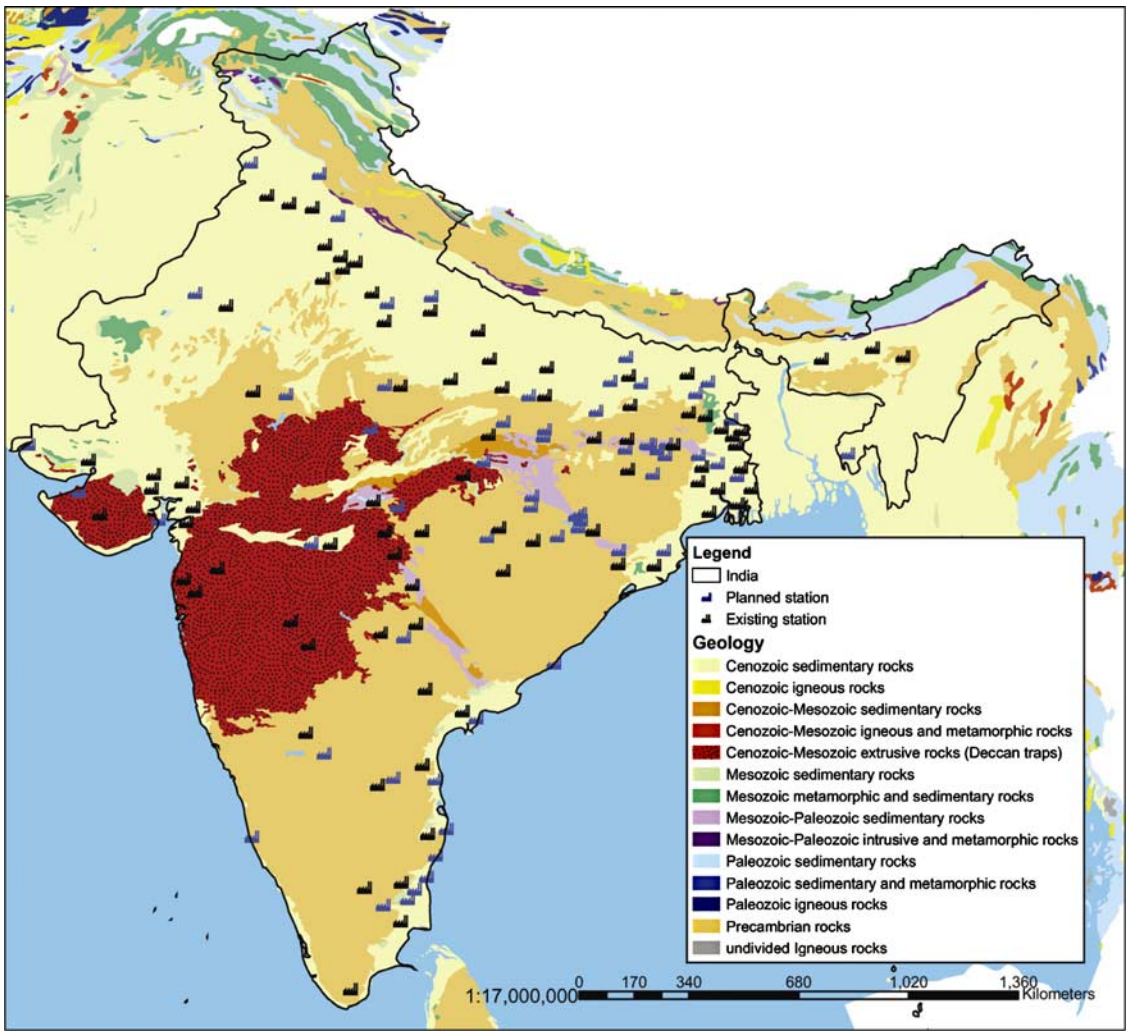

Figure 11. Distribution of existing (black) and planned (blue) coal-fueled power stations in India. The Deccan flood basalts are indicated in red located in the east central region of the country.

Peate, 1997] but India's Deccan Volcanic Province (DVP) is one of the largest terrestrial flood basalt formations, covering nearly 500,000 km^2 in west central India [*Eldholm and Coffin*, 2000; *Tiwari et al.*, 2001]. Origin of the DVP is generally viewed as an upwelling of a deep mantle plume beneath the Indian subcontinent dating back to the Cretaceous/Tertiary boundary [*Kennett and Widiyantoro*, 1999]. The DVP is composed of 13 different flows, typically of tholeiitic composition and consisting of massive, vesicular, amygdaloidal (small gas bubbles filled with secondary minerals) basalt tuff and breccia [*Tiwari et al.*, 2001; *Wignall*, 2001]. Interdispersed within the Deccan Trap flows are areas of well developed paleosols and lacustrine sediments that formed between eruptions. The DVP ranges in thickness from a few meters in the east to over 2.5 km in the west. Estimates of the DVP flow volume are about 512,000 km^3, which is nearly three times the size of the CRBG in the United States [*Eldholm and Coffin*, 2000]. The DVP is generally considered a seismically stable continental region, but seismic activity has been observed [*Reddy et al.*, 2000] and is an obviously important consideration that must be assessed with respect to geologic sequestration in any target formation.

[36] In addition to the DVP, a much smaller basalt formation in northeast India, the Rajmahal trap, consists of 450 to 600 m thick basalt covering an area of approximately 18,000 km^2. The Rajmahal basalts are commonly porphyritic with an unusually fine-grained matrix. The central part contains at least 28 lava flows of 20 to 70 m thickness [*Klootwijk*, 1971].

[37] Figure 11 shows the locations of existing and presently planned coal-fueled power plants in India. Of the total coal-fueled generation capacity in India (about 37 GW electric), 26% is located on or in close proximity to the Deccan basalts. This includes India's largest coal-fueled power plant, the Chandrapur facility in the Maharashtra district. The majority of the remaining plants are located on or near sedimentary formations that may also be suitable targets for geologic sequestration.

7. Conclusion

[38] Massive flood basalt formations exist in the United States and India that may be attractive for geologic sequestration of CO_2. Evidence from regional aquifer systems shows kilometer-scale interflow features with significant

porosity and lateral interconnectivity to support CO_2 injection. Low-permeability interbedded sediments and the impermeable basal rocks overlying each individual basalt flow may act as barriers to prevent CO_2 migration or at least slow the migration sufficiently to allow time for the mineralization reactions to occur. Calculations of basalt rock-water interactions indicate rapid rates of mineralization in pore water at equilibrium with supercritical CO_2 relative to typical sedimentary rocks. This time frame is short enough to enable validation in field pilot studies, if core samples can be obtained postinjection and located just under the CO_2 bubble where mixing of the CO_2 with the formation pore water would have occurred. At a much larger scale of importance for geologic sequestration, lateral dispersion and vertical transport of CO_2 to overlying basalt flows are expected to be important limiting factors in mineralization rates. Considerable additional work is needed to better understand the kinetics of these mineralization reactions as a function of temperature, CO_2 pressure, basalt composition, and especially the intra and interflow dispersion of CO_2 in basalts on a large scale.

[39] Although we have focused in this paper on the possibility of injecting CO_2 directly into basalt formations, it should also be noted that CO_2 could be injected into more conventional sedimentary formations that underlie basalt flows in some regions. For example, oil and gas exploration wells have been drilled recently through the basalts in eastern Washington State and in western India. Using more conventional sedimentary rock for injection could reduce uncertainty about siting and longevity of an injection field and still utilize the overlying basalt flow to absorb and eventually mineralize the CO_2 that migrates upward. As research continues to indicate a link between formation of vast igneous provinces and past global climate change events (including mass extinctions) [*Wignall*, 2001], it would indeed be ironic if these same geologic formations become an important part of the solution to the present-day greenhouse gas management challenge.

[40] **Acknowledgments.** The authors gratefully acknowledge the constrictive criticisms on the original manuscript offered by Stefan Bachu, Julio Friedmann, the Associate Editor, and several anonymous reviewers that greatly improved the final revision. This research was partially supported by Laboratory Directed Research and Development funding and by the U.S. Department of Energy, Office of Fossil Energy. The Pacific Northwest National Laboratory is operated by Battelle Memorial Institute for the U.S. Department of Energy under contract DE-AC05-76RL01830.

References

Aagaard, P., and H. C. Helgeson (1982), Thermodynamic and kinetic constraints on reaction rates among minerals and aqueous solutions. I. Theoretical considerations, *Am. J. Sci.*, *282*, 237–285.

Bachu, S. (2000), Sequestration of CO_2 in geological media: Criteria and approach for site selection in response to climate change, *Energy Conver. Manage.*, *41*, 953–970.

Bachu, S., and J. J. Adams (2003), Sequestration of CO_2 in geological media in response to climate change: Capacity of deep saline aquifers to sequester CO_2 in solution, *Energy Conver. Manage.*, *44*, 3151–3175.

Bishop, C. W., M. D. Knoll, and R. C. Hertzog (2004), Characterizing the hydraulic components of a contaminated basalt aquifer using borehole geophysical and hydrological methods, *Eos Trans. AGU*, *85*(17), Jt. Assem. Suppl., Abstract NS23A-03.

Brady, P. V., and S. R. Gislason (1997), Seafloor weathering controls on atmospheric CO_2 and global climate, *Geochim. Cosmochim. Acta*, *61*, 965–973.

Brennan, S. T., and R. C. Burruss (2003), Specific sequestration volumes: A useful tool for CO_2 storage capacity assessment, *U.S. Geol. Surv. Open File Rep.*, *03-0452*.

De Wit, A. (2004), Miscible density fingering of chemical fronts in porous media: nonlinear simulations, *Phys. Fluids*, *16*, 163–175.

Department of Energy (DOE) (1988), Site characterization plan, reference repository location, Hanford site, Washington, *DOE/RW-0164*, vol. 2, Washington, D. C.

Department of Energy (DOE) (2003), Notice of request for information on the department's plan to implement FutureGen, *Fed. Regist.*, p. 19521, Natl. Energy Technol. Lab., Washington, D. C.

Dooley, J. J., and M. A. Wise (2003), Retention of CO_2 in geologic sequestration formations: Desirable levels, economic considerations, and the implications for sequestration R&D, in *Proceedings of the Sixth International Conference on Greenhouse Gas Control Technologies*, edited by J. Gale and Y. Kaya, pp. 273–278, Elsevier, New York.

Early, T. O., G. D. Spice, and M. D. Mitchell (1986), A hydrochemical data base for the Hanford site, Washington, *Rep. SD-BWI-DP-061*, Rockwell Hanford Oper., Richland, Wash.

Edmonds, J. A., P. Freund, and J. J. Dooley (2001), The role of carbon management technologies in addressing atmospheric stabilization of greenhouse gases, in *Proceedings of the Fifth International Conference on Greenhouse Gas Control Technologies*, edited by D. J. Williams et al., pp. 46–51, CSIRO Publ., Collingwood, Victoria, Australia.

Eldholm, O., and M. F. Coffin (2000), Large igneous provinces and plate tectonics, in *The History and Dynamics of Global Plate Motions*, *Geophys. Monogr. Ser.*, vol. 121, edited by M. A. Richards et al., pp. 309–326, AGU, Washington, D. C.

Franks, S. G., and R. W. Forester (1984), Relationships among secondary porosity, pore fluid chemistry and carbon dioxide, in *Clastic Diagenesis*, edited by D. A. McDonald and R. C. Surdam, pp. 63–78, Am. Assoc. of Pet. Geol., Texas Gulf Coast Sect., Tulsa, Okla.

Gouze, P., and A. Coudrain-Ribstein (2002), Chemical reactions and porosity changes during sedimentary diagenesis, *Appl. Geochem.*, *17*, 39–47.

Greenberg, J., and M. Tomson (1992), Precipitation and dissolution kinetics and equilibria of aqueous ferrous carbonate vs temperature, *Appl. Geochem.*, *7*, 185–190.

Gupta, N., P. Wang, B. Sass, P. Bergman, and C. Byrer (2001), Regional and site-specific hydrogeologic constraints on CO_2 sequestration in the midwestern United States saline formations, in *Proceedings of the Fifth International Conference on Greenhouse Gas Control Technologies*, edited by D. J. Williams et al., pp. 385–390, CSIRO Publ., Collingwood, Victoria, Australia.

Hanson, A. L., and S. Mitchell (1977), Water Resources Management Program: Walla Walla River Basin, Water Resources Inventory Area no. 32, Dept. of Ecol., Olympia, Wash.

Hoffert, M. I., et al. (2002), Advanced technology paths to global climate stability: energy for a greenhouse planet, *Science*, *298*, 981–987.

Huang, K., and N. D. Opdyke (1998), Magnetostratigraphic investigations on an Emeishan basalt section in western Guizhou Province, China, *Earth Planet. Sci. Lett.*, *163*, 1–14.

Intergovernmental Panel on Climate Change (IPCC) (2005), IPCC special report on carbon dioxide capture and storage, Geneva, Switzerland.

Jensen, D. L., J. K. Boddum, J. C. Tjell, and T. H. Christensen (2002), The solubility of rhodochrosite ($MnCO_3$) and siderite ($FeCO_3$) in anaerobic aquatic environments, *Appl. Geochem.*, *17*, 503–511.

Johnson, J. W., J. K. Nitao, and K. G. Knaus (2004), Reactive transport modelling of CO_2 storage in saline aquifers to elucidate fundamental processes, trapping mechanisms, and sequestration partitioning, in *Geological Storage of Carbon Dioxide*, edited by S. J. Baines and R. H. Worden, *Geol. Soc. Spec. Publ.*, *233*, 107–128.

Kennett, B. L. N., and S. Widiyantoro (1999), A low seismic wavespeed anomaly beneath northwestern India—A seismic signature of the Deccan plume?, *Earth Planet. Sci. Lett.*, *165*, 145–155.

Kerr, R. C., and S. R. Tait (1985), Convective exchange between pore fluid and an overlying reservoir of denser fluid - A post-cumulus process in layered intrusions, *Earth Planet. Sci. Lett.*, *75*, 147–156.

Klootwijk, C. T. (1971), Paleomagnetism of the Upper Gondwana Rajmahal traps, northeast India, *Tectonophysics*, *12*, 449–467.

Knauss, K. G., J. W. Johnson, and C. I. Steefel (2005), Evaluation of the impact of CO_2, co-contaminant gas, aqueous fluid and reservoir rock interactions on the geologic sequestration of CO_2, *Chem. Geol.*, *217*, 339–350.

Kulkarni, H., S. B. Deolankar, A. Lalwani, B. Joseph, and S. Pawar (2000), Hydrogeological framework of the Deccan Basalt groundwater systems, west-central India, *Hydrogeol. J.*, *8*, 368–378.

Lackner, K. S., D. P. Butt, and C. H. Wendt (1997), Progress on binding CO_2 in mineral substrates, *Energy Conver. Manage.*, *38*, S259–S264.

Lemmon, E. W., M. O. McLinden, and D. G. Friend (2005), Thermophysical properties of fluid systems, in *NIST Chemistry WebBook, NIST Standard Reference Database Number 69*, edited by P. J. Linstrom and W. G. Mallard, Natl. Inst. of Stand. and Technol., Gaithersburg, Md. (Available at http://webbook.nist.gov)

Lico, M. S., and R. L. Seiler (1994), Ground-water quality and geochemistry, Carson Desert, western Nevada, *U.S. Geol. Surv. Open File Rep.*, *94-31*, 91 pp.

Lindeberg, E., and D. Wessel-Berg (1997), Vertical convection in an aquifer column under a gas cap of CO_2, *Energy Conver. Manage.*, *38*, S229–S234.

Luzier, J. E., and R. J. Burt (1974), Hydrology of basalt aquifers and depletion of ground water in east-central Washington, *Water Supply Bull. 33*, 53 pp., Wash. State Dep. of Ecol., Olympia.

MacNish, R. D., and R. A. Barker (1976), Digital simulation of basalt aquifer system, Walla Walla River Basin, Washington and Oregon, *Water Supply Bull. 44*, 51 pp., Wash. State Dep. of Ecol., Olympia.

McBride, J. H. (1991), Constraints on the structure and tectonic development of the early Mesozoic South Georgia Rift, southeastern United States: Seismic reflection data processing and interpretation, *Tectonics*, *10*, 1065–1083.

McGrail, B. P., M. D. White, P. F. Martin, and H. T. Schaef (2003), Mixing rates of supercritical CO_2 with brine in deep sedimentary formations, paper presented at Second National Conference on Carbon Sequestration, Exchange Monitor Publ. and Forums, Alexandria, Va.

O'Connor, W. K., D. C. Dahlin, G. E. Rush, C. L. Dahlin, and W. K. Collins (2002), Carbon dioxide sequestration by direct mineral carbonation: Process mineralogy of feed and products, *Miner. Metall. Processes*, *19*, 95–101.

Peate, D. W. (1997), The Paraná-Etendeka Province, in *Large Igneous Provinces: Continental, Oceanic, and Planetary Flood Volcanism*, *Geophys. Monogr. Ser.*, vol. 100, edited by J. J. Mahoney and M. F. Coffin, pp. 217–245, AGU, Washington, D. C.

Pokrovsky, O. S., and J. Schott (2000), Kinetics and mechanism of forsterite dissolution at 25°C and pH from 1 to 12, *Geochim. Cosmochim. Acta*, *64*, 3313–3325.

Pruess, K., and J. García (2002), Multiphase flow dynamics during CO_2 disposal into saline aquifers, *Environ. Geol.*, *42*, 282–295.

Puffer, J. H., and R. A. Volkert (2001), Pegmatoid and gabbroid layers in Jurassic Preakness and Hook Mountain basalts, Newark Basin, New Jersey, *J. Geol.*, *109*, 585–601.

Puffer, J. H., D. O. Hurtubise, F. J. Geiger, and P. Lechler (1981), Chemical-composition and stratigraphic correlation of Mesozoic basalt units of the Newark Basin, New-Jersey, and the Hartford Basin, Connecticut: Summary, *Geol. Soc. Am. Bull.*, *92*, 155–159.

Reddy, C. D., G. El-Fiky, T. Kato, S. Shimada, and K. V. Kumar (2000), Crustal strain field in the Deccan Trap region, western India, derived from GPS measurements, *Earth Planets Space*, *52*, 965–969.

Reidel, S. P., V. G. Johnson, and F. A. Spane (2002), Natural gas storage in basalt aquifers of the Columbia Basin, Pacific Northwest USA: A guide to site characterization, *Rep. PNNL-13962*, Pac. Northwest Natl. Lab., Richland, Wash.

Retallack, G. J. (2002), Carbon dioxide and climate over the past 300 Myr, *Philos. Trans. R. Soc. London Ser. A*, *360*, 659–673.

Saar, M. O. (1998), The relationship between permeability, porosity, and microstructure in vesicular basalts, Masters thesis, 91 pp, Univ. of Oreg., Eugene.

Saar, M. O., and M. Manga (1999), Permeability-porosity relationship in vesicular basalts, *Geophys. Res. Lett.*, *26*, 111–114.

Sahagian, D. L., and J. E. Maus (1994), Basalt vesicularity as a measure of atmospheric-pressure and palaeoelevation, *Nature*, *372*, 449–451.

Sahagian, D. L., A. T. Anderson, and B. Ward (1989), Bubble coalescence in basalt flows—Comparison of a numerical-model with natural examples, *Bull. Volcanol.*, *52*, 49–56.

Sass, B. M., M. H. Engelhard, P. Bergman, and C. Byrer (2001), Interaction of rock minerals with carbon dioxide and brine: A hydrothermal investigation, paper presented at First National Conference on Carbon Sequestration, Natl. Energy Technol. Lab., Washington, D. C., 14 –17 May.

Seidemann, D. E., W. D. Masterson, M. P. Dowling, and K. K. Turekian (1984), K-Ar dates and $^{40}Ar/^{39}Ar$ age spectra for Mesozoic basalt flows of the Hartford Basin, Connecticut, and the Newark Basin, New Jersey, *Geol. Soc. Am. Bull.*, *95*, 594–598.

Shin, H., W. B. Lindquist, D. L. Sahagian, and S. R. Song (2005), Analysis of the vesicular structure of basalts, *Comput. Geosci.*, *31*, 473–487.

Song, S. R., K. W. Jones, W. B. Lindquist, B. A. Dowd, and D. L. Sahagian (2001), Synchrotron X-ray computed microtomography: Studies on vesiculated basaltic rocks, *Bull. Volcanol.*, *63*, 252–263.

Tajika, E. (1998), Climate change during the last 150 million years: Reconstruction from a carbon cycle model, *Earth Planet. Sci. Lett.*, *160*, 695–707.

Tiwari, V. M., M. B. S. Vyaghreswara Rao, and D. C. Mishra (2001), Density inhomogeneities beneath Deccan Volcanic Province, India as derived from gravity data, *Geodynamics*, *31*, 1–17.

Tomkeieff, S. I. (1940), The basalt lavas of Giant's Causeway, District of Northern Ireland, *Bull. Volcanol.*, *6*, 89–143.

U.S. Geological Survey (USGS) (1999), *Ground Water Atlas of the United States*, Reston, Va.

Varekamp, J. C., R. Kreulen, R. P. E. Poorter, and M. J. Vanbergen (1992), Carbon-sources in arc volcanism, with implications for the carbon-cycle, *Terra Nova*, *4*, 363–373.

Wels, C., S. Shaw, and M. Royle (2000), A case history of intrinsic remediation of reactive tailings seepage for Questa Mine, New Mexico, paper presented at ICARD 2000 Conference, Soc. of Min., Metall., and Explor., Inc., Denver, Colo.

Westrich, H. R., R. T. Cygan, W. H. Casey, C. Zemitis, and G. W. Arnold (1993), The dissolution kinetics of mixed-cation orthosilicate minerals, *Am. J. Sci.*, *293*, 869–893.

White, M. D., and B. P. McGrail (2005), Numerical simulation of CO_2 injection and sequestration in saline and hydrate bearing aquifers, paper presented at Fourth Annual Conference on Carbon Capture and Sequestration, U.S. Dep. of Energy, Alexandria, Va.

Wigley, T. M. L., R. Richels, and J. A. Edmonds (1996), Economic and environmental choices in the stabilization of atmospheric CO_2 concentrations, *Nature*, *379*, 240–243.

Wignall, P. B. (2001), Large igneous provinces and mass extinctions, *Earth Sci. Rev.*, *53*, 1–33.

Wilke, H. (1995), Interaction of traveling chemical waves with density driven hydrodynamic flows, *Physica D*, *86*, 508–513.

Wogelius, R. A., and J. V. Walther (1991), Olivine dissolution at 25°C: Effects of pH, CO_2, and organic acids, *Geochim. Cosmochim. Acta*, *55*, 943–954.

Wogelius, R. A., and J. V. Walther (1992), Olivine dissolution kinetics at near-surface conditions, *Chem. Geol.*, *97*, 101–112.

Wolery, T. J. (1992), EQ3NR, A computer program for geochemical aqueous speciation-solubility calculations: Theoretical manual, user's guide, and related documentation, version 7.0, *Rep. UCRL-MA-110662 PT III*, Lawrence Livermore Natl. Lab., Livermore, Calif.

Xu, T. F., J. A. Apps, and K. Pruess (2004), Numerical simulation of CO_2 disposal by mineral trapping in deep aquifers, *Appl. Geochem.*, *19*, 917–936.

Xu, T. F., J. A. Apps, and K. Pruess (2005), Mineral sequestration of carbon dioxide in a sandstone-shale system, *Chem. Geol.*, *217*, 295–318.

Zhang, Y. P., and R. A. Dawe (2000), Influence of Mg^{2+} on the kinetics of calcite precipitation and calcite crystal morphology, *Chem. Geol.*, *163*, 129–138.

Y.-J. Chien, B. P. McGrail, and H. T. Schaef, Applied Geology and Geochemistry Department, Pacific Northwest National Laboratory, P.O. Box 999, Richland, WA 99352, USA. (pete.mcgrail@pnl.gov)

C. L. Davidson, Technology Systems Analysis Department, Pacific Northwest National Laboratory, P.O. Box 999, Richland, WA 99352, USA.

J. J. Dooley, Joint Global Change Research Institute, Pacific Northwest National Laboratory, College Park, MD 20742, USA.

A. M. Ho, Department of Geology, Flathead Valley Community College, Kalispell, MT 59901, USA.